*Article*

# Poly(vinyl alcohol)-Based Electrospun Nanofibers with Improved Antimicrobial Activity

*Paola A. P. Machado,[a] Gabriel N. Fraga,[a] Alessandra R. Medeiros,* [a]
*Michelly C. G. Pellá,* [b] *Nelson B. Colauto,[c] Giani A. Linde,[c] Fernando N. Cavalheiro,[d]*
*Maria G. I. Faria,[d] Douglas C. Dragunski* [a] *and Josiane Caetano* *,[a]

[a]*Grupo Interdisciplinar de Pesquisa em Fotoquímica e Eletroquímica Ambiental (GIPeFEA),
Departamento de Química, Universidade Estadual do Oeste do Paraná (Unioeste),
85903-000 Toledo-PR, Brazil*

[b]*Grupo de Materiais Poliméricos e Compósitos (GMPC), Departamento de Química,
Universidade Estadual de Maringá, Av. Colombo, 5790, 87020-900 Maringá-PR, Brazil*

[c]*Programa de Pós-Graduação em Ciência dos Alimentos, Universidade Federal da Bahia, 147,
40170-115 Salvador-BA, Brazil*

[d]*Programa de Pós-Graduação em Biotecnologia Aplicada à Agricultura,
Universidade Paranaense (Unipar), 87502-210 Umuarama-PR, Brazil*

Electrospinning was used to produce poly(vinyl alcohol) (PVA)-based nanofibers containing nerolidol (NER) as the antimicrobial agent. The scanning electron microscopy results indicated the formation of homogeneous fibers in the absence of NER. However, its incorporation into the fiber prevented the complete solvent evaporation, ultimately leading to the coalescence of the fibers. It became more evident as the amount of NER increased from 0 to 50% m/v. The incorporation of NER also decreased the crystallinity of the fibers from 10 to ca. 6.5%. However, this decrease was not proportional to the concentration of NER. The contact angle results confirmed the presence of NER molecules on the surface of the fibers especially due to the increase of the contact angle from 0 (PVA/NER0) to 27.8° (PVA/NER50). The fibrous mats exhibited good antimicrobial activity, being even more efficient than the control in some cases, suggesting their potential for wound-dressing purposes.

**Keywords:** wound dressing, monoaxial electrospinning, emulsion electrospinning, biomaterial

## Introduction

Biomaterials have been used for a wide variety of purposes. The literature reports their use as drug delivery systems,[1-3] scaffolds for tissue engineering,[4,5] packaging and coatings for food,[6-8] and for the protection of topic wounds,[9,10] for example.

The materials aimed at the protection of topic wounds are called wound dressings. Initiating wound healing, preventing external contamination, and removing excess of exudates are some of the main goals regarding wound dressings.[11] The dressings can be produced by self-assembly,[12] dry/wet-phase inversion,[13] and

bioprinting.[14] However, the electrospinning method is probably the most preferred one.[15-19] The relative simplicity and efficiency of electrospinning in producing polymer-based fibers might be the reasons behind the preference for this method over the other ones.

Synthetic and natural polymers are suitable for fiber production using the electrospinning technique.[20] Nevertheless, although natural polymers have the pros of being biocompatible and biodegradable, their variability represents a significant drawback and often limits their use.[21] Besides the regular and reproducible structure,[22,23] synthetic polymers like polyamides, polyacrylates, and polyesters are also biocompatible,[21] making them attractive for the production of electrospun-based wound dressings.

Polyvinyl alcohol (PVA) is a non-toxic,[24] non-carcinogenic, and biocompatible[24] synthetic polymer

suitable for the production of fibers using the electrospinning technique,[25] leading to mechanically resistant and non-adhesive fibers.[26] Moreover, the ability to swell water displayed by PVA allows the fibers to absorb exudates and to keep the wounded area hydrated.[26] Besides the advantages mentioned above, the water solubility of PVA allows its dissolution in aqueous heated mediums.[27]

Despite its advantages, PVA does not display antimicrobial activity. However, the incorporation of bioactive agents, like nerolidol, could easily overcome this limitation. Nerolidol (3,7,11-trimethyl-1,6,10-dodecatrien-3-ol, NER)[28] is a sesquiterpene alcohol commonly found in essential oils obtained from sour orange (*Citrus aurantium* L.), ginger (*Zingiber officinale* Roscoe), lavender (*Lavandula angustifolia* Mill.) and lemon grass (*Cymbopogon citratus* (DC.) Stapf).[28,29]

Nerolidol plays an active role in the defense system of some plants and has been explored by researchers for its antimicrobial, antifungal,[30] antibiofilm, antioxidant, anti-inflammatory activities,[28] and skin penetration enhancer.[28,31] The antimicrobial activity of nerolidol has been attributed to the hydrophobicity of this compound. Thus, it easily crosses the plasma membrane interacting with intracellular proteins and/or intra-organelle sites, causing the death of the bacteria cell.[32] Studies[29,30] have shown that nerolidol has antimicrobial activity against *Staphylococcus aureus* and *Salmonella enterica*, evidencing its potential against Gram-positive and Gram-negative bacteria.

In light of the pieces of information above, this work employed the electrospinning technique to produce a nanofibrous wound dressing based on PVA and evaluated if the incorporation of NER would improve their antimicrobial activity. Assessing the effect of NER on other characteristics of the fibers (i.e., morphology, crystallinity, hydrophobicity, and stability) was also a goal of this work.

## Experimental

### Materials

Nerolidol *cis* and *trans* mixture (NER, purity ≥ 97%) and poly(vinyl) alcohol (PVA; molecular weigth ($M_w$) 146-186 kg mol$^{-1}$, 99% hydrolyzed) were acquired from Sigma-Aldrich (Burlington, United States of America (USA)). Ethanol (99.8% P.A) was acquired from Neon (Suzano, Brazil). Sodium chloride (NaCl, 99%) was acquired from Reatec (São Paulo, Brazil). Penicillin G (PEN) and chloramphenicol (CLO) were purchased from Laborclin (Pinhais, Brazil). Mueller Hinton Agar was acquired from Kasvi (São José dos Pinhais, Brazil). All the reactants were used as received.

### Methods

#### Preparation of the electrospinning emulsion

Initially, PVA (8% m/v) was dissolved in 9 mL of distilled water under constant and vigorous magnetic stirring. The beaker was kept in a water bath at 80 °C until complete homogenization. After cooling to room temperature, the PVA solution was slowly added to 1 mL of ethanol 10% v/v to prevent polymer precipitation. The solution was magnetically stirred until homogenization. The respective amount of NER (0, 25, or 50% m/v) was added to the homogenized PVA ethanolic solution, and the mixture was magnetically stirred until the formation of an emulsion.

The emulsion was subsequently transferred to a glass syringe and electrospun using a potential of the applied voltage of 10 kV, a needle-to-collector distance of 18 cm, and a flow rate of 1 mL h$^{-1}$. The fibers were produced at relative air humidity ranging between 30 and 40%.

The obtained fibrous mats were named PVA/NERx, in which PVA/NER refer to the precursors used to produce them (poly(vinyl alcohol) and nerolidol), and "x" specifies the amount of NER used to produce the fiber (x = 0, 25, or 50% m/v).

### Characterization of membranes

#### Scanning electron microscopy (SEM)

The morphology of the fibers was determined by SEM analysis. The samples were fixed in double-sided carbon tape (placed on a stub) and coated with gold (30 nm-thick gold film) using the cathodic deposition method (BAL-TEC-SCD 050). The analysis was performed in a QUANTA 250 equipment (Hillsboro, USA), operating at a voltage of 20 kV.

The SEM micrographs were used to determine the diameter of the fibers. The measures were performed using the software ImageJ,[33] in random parts of each sample, totaling one hundred measures (n = 100). The results are expressed by mean ± standard deviation (SD; mean ± SD).

#### Fourier infrared spectroscopy with attenuated total reflectance (FTIR-ATR)

The analysis of Fourier transform infrared spectroscopy with attenuated total reflectance (FTIR-ATR) was performed using the PerkinElmer Frontier spectrophotometer (Waltham, USA). Each spectrum is the result of 8 scans from 4000 to 600 cm$^{-1}$, at a resolution of 2 cm$^{-1}$.

The obtained data were processed (baseline subtraction and data normalization) using data processing software. The results are expressed in arbitrary units (a.u.).

### X-ray diffraction (XRD)

The diffraction pattern of the PVA/NERx samples was determined by X-ray diffraction using a D2 Phaser Bruker® equipment (Billerica, USA). The experimental conditions were: a Cu Kα radiation source (λ = 1.5418 Å), an operating voltage of 40 kV voltage and a current of 30 mA, using a graphite monochromator. The patterns were assessed between 2θ = 10° and 2θ = 80°, with an increment of 0.02° min⁻¹.

The obtained data were processed (smoothing, baseline subtraction, and data normalization) using data processing software. The results are expressed in arbitrary units (a.u.).

### Contact angle

The contact angle was measured in a USB microscope connected to a computer. A drop of distilled water (5 μL) was deposited on the surface of the fibrous mat and monitored for 5 min.

The measure was performed in duplicate (n = 2). The drop was placed in a random part of the mat, and a new piece of the mat was used for each replicate. They were acquired at a magnification of ten times, and the contact angle was determined using the ImageJ software.[33] The results are expressed by mean ± SD.

### Differential scanning calorimetry (DSC)

The DSC analysis was performed in a Shimadzu DSC-60 Thermal Analyzer (Kyoto, Japan). The samples (ca. 6 mg) were placed in aluminum crucibles, and heated from 30 to 250 ºC (and cooled from 250 to 30 °C) at a rate of 10 ºC min⁻¹, under an $N_2$ atmosphere (flow rate of 50 mL min⁻¹).

The enthalpy of the thermal events observed in the thermograms was calculated by integrating the curves. The integration was performed using an end-points straight line as the baseline.

The percentage of crystallinity ($X_c$) of the fibers was determined from the DSC data, using equation 1,[34] in which $\Delta H_f$ and $\Delta H_{cc}$ describe, respectively, the enthalpy of melting and cold crystallization of the fibers, and $\Delta H_f^0$ is the heat of fusion of completely crystalline PVA ($\Delta H_f^0 = 141.83$ J g⁻¹ for PVA).[35]

$$X = \frac{\Delta H_f^0 - \Delta H_{cc}}{\Delta H_f^0} \times 100 \qquad (1)$$

### Thermogravimetric analysis (TG/DTG)

Thermal stability was evaluated by thermogravimetric analysis (TGA) in a PerkinElmer STA 6000 thermal analyzer (Waltham, USA) using ceramic cells. For the analysis, ca.10 mg of each sample was heated from 25 to 600 ºC (heating rate of 10 ºC min⁻¹) under an $N_2$ atmosphere (flow rate of 50 mL min⁻¹). The first derivate (DTG) was obtained using data processing software.

### Antimicrobial activity

The antimicrobial activity of the films was determined following the disc diffusion method, based on the Clinical and Laboratory Standards Institute (CLSI) with modifications (CLSI, 2019).[36] The antimicrobial activity of the PVA/NERx fibrous mats was assessed against the bacteria *Staphylococcus aureus* subsp. *aureus*, ATCC 29213™, *Staphylococcus epidermidis* (Winslow and Winslow) Evans, ATCC 12228™, and *Pseudomonas aeruginosa* (Schroeter) Migula, ATCC 27853™.

Colonies from a 24 h-culture at 35 °C in a growth medium were added with a bacterial inoculating loop to sterile saline (0.85% NaCl) until obtaining turbidity compatible with the 0.5 Mcfarland standard (1.5 × 10⁸ colony forming units (CFU) mL⁻¹), without the need for incubation. The concentration of microorganisms in the inoculum was confirmed in a spectrophotometer at 625 nm with absorbance ranging from 0.08 to 1.0.

After the inoculum preparation, a sterile swab was soaked in the bacterial suspension, removing the excess by pressing the swab against the walls of the tube. It was gently streaked in at least 5 directions in a Petri dish containing Mueller Hinton Agar, covering the entire surface. With the aid of a flamed and cooled tweezer, discs of the PVA/NERx mats (diameter of 0.8 mm) were added to the surface of the inoculated medium. The dishes were subsequently incubated in a bacteriological oven at 35 °C for 24 h. Discs of penicillin G (10 μg) and chloramphenicol (30 μg) were used as the positive control. The inhibition zone diameter of each disc was measured with the aid of a millimeter ruler. The experiment was carried out in triplicate (n = 3), and the results are expressed by mean ± SD.

### *In vitro* stability assay

The stability assay was performed by placing the samples (of known masses) in beakers containing 25 mL of phosphate buffer solution (pH 5.47). The beakers were orbitally stirred (100 rpm) for 24 h at 35 °C.

The samples were removed from the aqueous medium after 24 h; transferred into a desiccator for another 24 h, and weighed in an analytical balance. The analysis was performed in triplicate (n = 3), and the results are expressed by mean ± SD.

### Statistical analysis

The obtained data were subjected to statistical analysis whenever possible. The results were assessed by analysis

of variance (ANOVA), Tukey's test, and *t*-test, at 95% of significance using the software Minitab 19.[37]

## Results and Discussion

### Morphology

The morphological characteristics of the membranes were evaluated using SEM analysis. Figure 1 displays the results that confirm the formation of nanofibrous structures for the electrospun PVA solutions, with and without NER. The solution containing only PVA (PVA/NER0; Figure 1a) led to homogeneous fibers of smooth surfaces. This condition also led to bead-free fibers, which are attractive for electrospun-based materials because bead-free fibers are more prone to exhibit the same characteristic throughout their extension.[20]

The incorporation of NER into the polymeric solution changed the characteristic of the fibers, especially for PVA/NER50. The SEM micrographs of this sample in Figure 1c suggest the coalescence of the fibers. The non-polar nature of NER might explain this behavior. Since they have opposite polarities (PVA is polar[38] and NER is non-polar), it is possible that the van der Waals interactions formed between them were very weak.[39] It allows one to hypothesize that the fibers had regions formed by a few NER molecules surrounded by a lot of

PVA molecules. The regions containing the NER molecules probably had a different solvent evaporation rate. In this case, the needle-to-collector distance was probably too small to allow complete solvent evaporation. If the fibers are still wet when reaching the collector, they inevitably coalesce. The higher homogeneity of the PVA/NER25 fibers (Figure 1b) reinforces this hypothesis. However, it is not possible to establish whether there was a concentration of NER molecules in isolated regions of the fibers based on SEM results only.

The incorporation of NER also affected the diameter of the fibers. Table 1 presents the obtained values, which were determined from the SEM micrographs. The diameter ranged from (583 ± 144) to (901 ± 193) nm for samples PVA/NER25 and PVA/NER50, respectively. As mentioned before, PVA and NER have opposite polarities. The combination of substances of such different polarities usually decreases the surface tension of the solution.[40] Up to a certain level, lower surface tensions are attractive to the electrospinning technique because they facilitate the ejection of the polymeric solution and its whipping until the collector.[20,41,42] However, lower surface tension is only beneficial up to a critical level. Below this level, the electrospinning reaches an unstable state, and the produced fibers do not necessarily obey theoretical behaviors. This might be why the PVA/NER25 fibers were thinner than the PVA/NER0 ones.
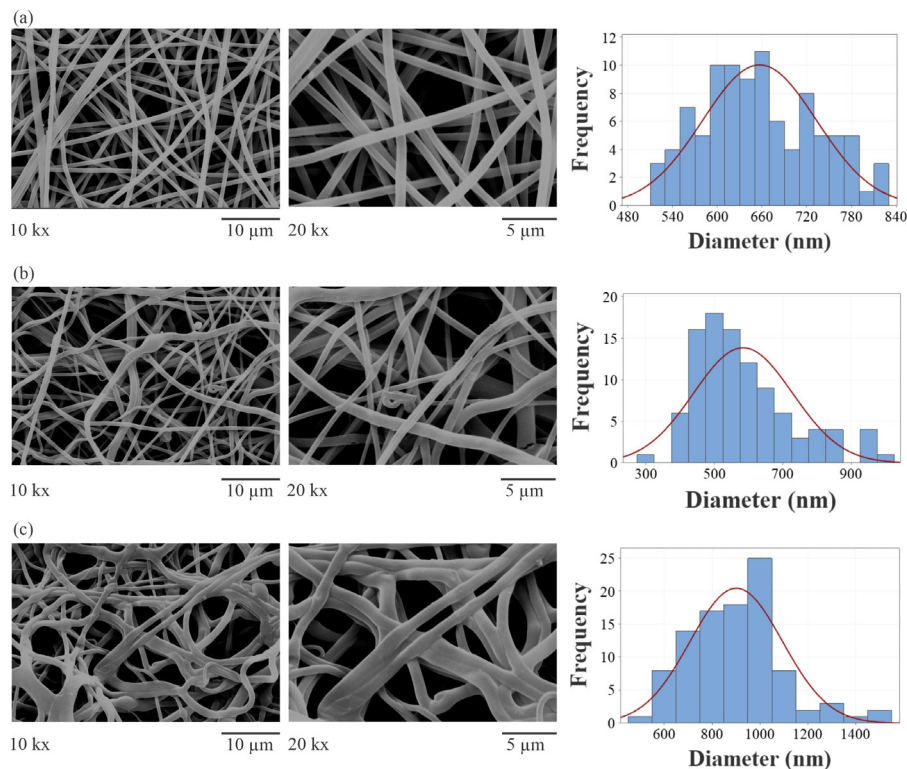


**Figure 1.** SEM micrographs and normal distribution plots regarding the diameter of (a) PVA/NER0, (b) PVA/NER25, and (c) PVA/NER50.

**Table 1.** Mean diameter of the PVA/NERx fibers, measured from the SEM micrographs

| Sample | Diameter / nm |
| --- | --- |
| PVA/NER0 | 656 ± 76.4[a] |
| PVA/NER25 | 583 ± 144[b] |
| PVA/NER50 | 901 ± 193[c] |

(Mean ± SD) that do not share the same letter are statistically different at 95%. The values were standardized to three significant figures.

It is also possible that NER molecules were entrapped inside the jet as it was ejected from the needle. The molecules of different polarities might have repelled each other. It would force the molecules to get as apart from each other as possible to minimize the repulsive forces, ultimately leading to fibers of larger diameters. It might explain the larger diameter of the PVA/NER50 fibers compared to the other ones.

The standard deviation of the diameters increased as the amount of NER increased, and statistical analysis confirmed that all samples were statistically different regarding their diameter. The polarity difference likely prevented the formation of a homogeneous solution. The literature states that higher conductivities aid the formation of the Taylor cone.[20,43] Hence, the dispersity of the diameters throughout the fibers might be the result of different conductivities caused by the low (yet existing) NER dissolution in the PVA ethanolic solution.

Bruni *et al*.[44] also observed the coalescence of their fibers. They used emulsion-electrospinning to encapsulate β-carotene into PVA/soy protein isolate-based fibers, and electrospun onto polyhydroxybutyrate-co-valerate films. In their case, the coalescence became more evident after exposing the material to an annealing treatment.

### Physical-chemical characterization

FTIR and XRD analyses were used as tools to evaluate if PVA and NER interacted with each other, and how did their combination affect the produced fibers. Figure 2 depicts a schematical representation of the interactions observed in the fibers, the FTIR, and the XRD results. Both precursors (PVA and NER) can interact via polar and non-polar interactions. The presence of oxygen atoms in both precursors allows the formation of van der Waals interactions between the carbon backbone of PVA and the carbon atoms from NER. Moreover, both have hydroxyl (OH) groups in their structure, allowing the formation of hydrogen bonds between the species.

The FTIR spectra of pure PVA display a characteristic OH band at 3333 cm$^{-1}$ (symmetrical stretching). The bands at 2939, 2901 (symmetrical), and 2837 cm$^{-1}$ (asymmetrical) match the stretching of CH sp$^3$, and the band at 1420 cm$^{-1}$ describes the bending vibration of CH$_2$. The stretching of the C–O band is responsible for the band at 1089 cm$^{-1}$, and the 1% of non-hydrolyzed PVA from the matrix explains the ester carbonyl band (CH$_3$O–C=O) at 1736 cm$^{-1}$.[45,46]

The FTIR spectra of pure NER also present characteristic OH bands at 3402 cm$^{-1}$. The bands between 2966 and
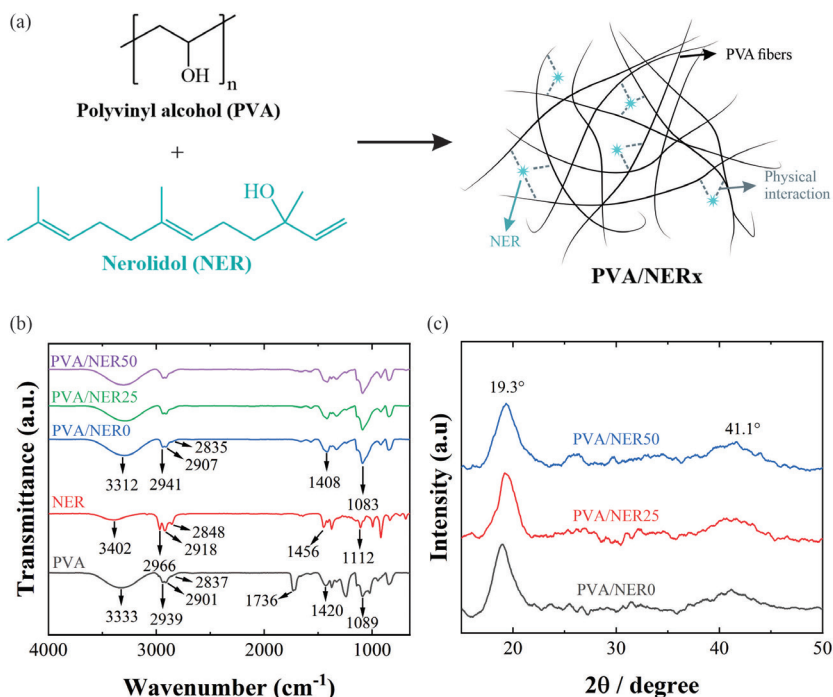


**Figure 2.** (a) Schematic representation of the interaction in the fibers, (b) FTIR-ATR spectra, and (c) XRD diffractograms of the PVA/NER-based samples.

2848 cm$^{-1}$ are the result of the stretching of C–H sp$^3$ bonds. Even though the FTIR spectra do not present any C–H sp$^2$ band at wavenumbers higher than 3000 cm$^{-1}$, probably due to the overlapping with the OH band, the band at 1456 cm$^{-1}$ matches the bending of CH sp$^2$.[45] The band at 1112 cm$^{-1}$ is characteristic of the stretching of C–O bonds.

The fibers presented bands from both precursors regardless of their amount. However, the bands shifted to smaller wavenumbers in the PVA/NERx fibers. Even though it could be a result of the formation of physical intermolecular interactions (London and van der Waals forces, and hydrogen interactions) between the precursors, it could also indicate that the electrospinning process itself already changes the dynamic of the forces experienced by the polymer.

The FTIR results do not indicate the formation of chemical bonds between PVA and NER. This reaction would only be possible at the non-hydrolyzed PVA portions. However, the reaction between the hydroxyl group (OH) from NER with the ester carbonyl group from PVA would rely on an acid or base catalyst, or on an extreme environment (the use of high temperature, for example) to force the addition-elimination reaction to occur.[47,48] Since neither catalysts nor high temperatures were employed in the process, the formation of a chemical bond between the species was very unlikely to happen. The absence of bands at wavenumbers lower than 1730 cm$^{-1}$ supports the previous statement.[45]

The XRD results (Figure 2c) suggest a slight change in the center of the first peak ($2\theta$ ca. 19.3°). This peak, attributed to the crystallographic plane (101) of the crystalline part of PVA,[49,50] was centered at $2\theta = 18.9°$ for PVA/NER0 and shifted to $2\theta = 19.3°$ to PVA/NER25 and PVA/NER50. Nevertheless, the center of the peak did not change as the amount of NER increased. It suggests that, despite the very little effect of NER on PVA, they do interact with each other (probably via van der Waals and London forces, and hydrogen interaction).

## Contact angle

The polarity of the surface of the fibers was evaluated by contact angle measures. Table 2 displays the results. As mentioned before, PVA is a hydrophilic polymer.[38] Its fibers absorbed the drop of water immediately after it touched the surface of the fibers. Consequently, the contact angle of the PVA/NER0 fibers was 0°.

The hydrophobic character of NER affected the surface polarity of the fibers, increasing the contact angle to $(27.8 \pm 0.27)°$ for the fibers containing the highest amount of NER (PVA/NER50). Even though the contact angle

increased only 1.3 times from PVA/NER25 to PVA/NER50, all matrices were statistically different at 95% according to Tukey's test.

**Table 2.** The contact angle of the PVA/NERx fibers, assessed by the sessile drop method

| Sample | Contact angle / degree |
|---|---|
| PVA/NER0 | $0.00 \pm 0.00^a$ |
| PVA/NER25 | $20.9 \pm 1.34^b$ |
| PVA/NER50 | $27.8 \pm 0.27^c$ |

(Mean ± SD) that do not share the same letter are statistically different at 95%. The values were standardized to three significant figures.

The contact angle results indicate the presence of NER molecules on the outer parts of the fibers. However, it is not possible to establish whether NER (*i*) coated the entire surface of the fibers, (*ii*) coated narrow regions, or (*i*) randomly distributed on their surface based on these results. They merely confirm the presence of NER on the surface of the fibers, and that the concentration of NER molecules on their surface increases by increasing the amount of NER in the blend.

## Thermal stability

DSC and TGA were used to evaluate if the incorporation of NER would affect the thermal stability of the fibers. Figure 3 depicts the results. The PVA/NER0 fibers (Figure 3a) exhibited a broad peak centered at 79 °C. It is the result of the loss of adsorbed water molecules[50,51] and the reorganization of flexible chains as a result of the melting of crystalline regions from PVA.[52] According to the TG/DTG results, it led to a mass loss of 6.80%. The second event (peak 2) describes the temperature of melting (Tm) of PVA.[53,54] The increase in temperature leads to the decomposition of side chains (dihydroxylation of PVA),[49,55] being responsible for a mass loss of 71.4%, as observed in the TG/DTG thermogram. Finally, at 371 °C, conjugated cyclic by-products were degraded into carbonized residues.[51,56] The third DSC peak (peak 3; 179 °C) matches the temperature of cold crystallization ($T_{cc}$) of PVA.

The matrices containing NER presented the same peaks observed for PVA/NER0, but the results evidence the influence of NER on the structure of the fibers, confirming the FTIR and XRD suggestions of interaction between PVA and NER. The events observed in the DSC thermograms became broader and less resolved as the amount of NER increased from 25 (Figure 3b) to 50% (Figure 3c). Furthermore, the center of the second endothermic event shifted from 79.1 °C (PVA/NER0) to 66.0 °C (PVA/NER50).
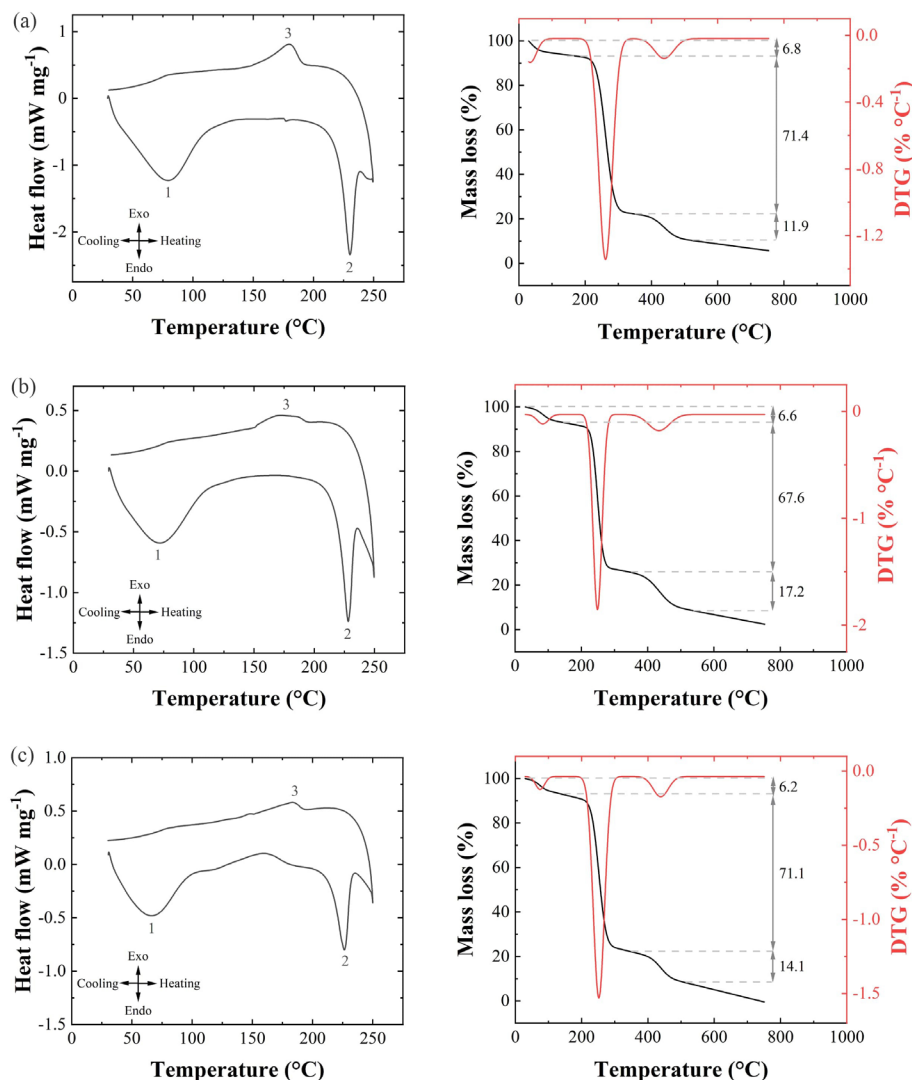
**Figure 3.** DSC (left side) and TG/DTG (right side) of (a) PVA/NER0, (b) PVA/NER25, and (c) PVA/NER50.

Furthermore, peak 1 became less intense as the amount of NER increased. It is the result of the higher hydrophobicity of the fibers, as confirmed by the contact angle measures, which decreases the adsorption of water molecules. Moreover, these results suggest that the fibers became less crystalline and thermally stable as the amount of NER increased. The percentage of crystallinity results presented in Table 3 supports this statement.

The crystallinity results confirm that NER decreased $X_c$. However, unlike suggested by the SEM micrographs (Figure 1), the crystallinity of PVA/NER25 and PVA/NER50 was very similar. Considering all the already presented and discussed results, it is possible to infer that the addition of NER impairs the evaporation of the solvent and ultimately leads to the coalescence of the fibers. It does decrease their crystallinity (compared to PVA/NER0). However, even

**Table 3.** The temperatures of water loss ($T_w$), melting ($T_m$), and cold crystallization ($T_{cc}$), the respective enthalpy ($\Delta H$) for each process (water loss, $\Delta H_w$, melting, $\Delta H_m$, and cold crystallization, $\Delta H_{cc}$), and the percentage of crystallinity ($X_c$) for the PVA/NERx fibers

| Sample | Peak 1 | | Peak 2 | | Peak 3 | | $X_c$ / % |
|---|---|---|---|---|---|---|---|
| | $T_w$ / °C | $\Delta H_w$ / (J g$^{-1}$) | $T_m$ / °C | $\Delta H_m$ / (J g$^{-1}$) | $T_{cc}$ / °C | $\Delta H_{cc}$ / (J g$^{-1}$) | |
| PVA/NER0 | 79.1 | 61.7 | 230 | 6.01 | 179 | −8.37 | 10.1 |
| PVA/NER25 | 72.3 | 33.5 | 228 | 6.38 | 172 | −2.64 | 6.36 |
| PVA/NER50 | 66.0 | 21.1 | 226 | 8.28 | 183 | −1.64 | 7.00 |

The values were standardized to three significant figures.

though the enthalpies of all events but $\Delta H_m$ for PVA/NER50 decreased as the amount of NER increased, the $X_c$ was not proportionally affected by the amount of NER.

Tampau *et al.*[57] also observed crystallinity decreases in PVA-based electrospun nanofibers. The fast solvent evaporation and polymer solidification, and the formation of metastable structures were the motives pointed out by the authors.

Antimicrobial activity

As mentioned in the Introduction section, NER has, among others, antimicrobial activity while the literature reports no such effect for pure PVA. The antimicrobial activity of the produced PVA/NERx fibers was assessed using the disc diffusion method, as described in the Experimental section. Figure 4 depicts the bacterial growth on the PVA/NERx fibers.
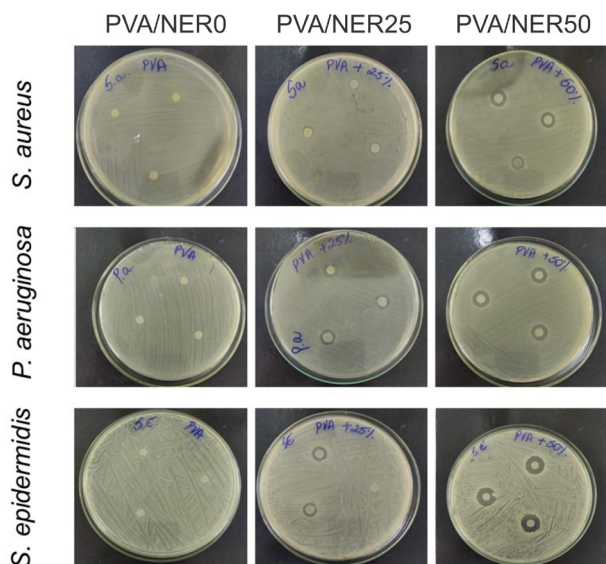


**Figure 4.** Antimicrobial of (a) PVA/NER0, (b) PVA/NER25, and (c) PVA/NER50 against *S. aureus*, *P. aeruginosa*, and *S. epidermidis*.

Table 4 presents the diameter of the inhibition zones, which confirms that PVA/NER0 was completely ineffective

in inhibiting the proliferation of microorganisms, leading to an inhibition zone of 0 mm. The fibers containing NER, on the other hand, were very effective in preventing microbial proliferation, especially at higher concentrations of NER.

The effectiveness of the fibers against microbial growth varied from one bacterium to another. For example, PVA/NER50 presented an inhibition zone of ($21.3 \pm 0.60$) mm for *Staphylococcus epidermidis*. This result suggests that this fiber is even more effective than penicillium (used as one of the controls). The same effect was observed against *Staphylococcus aureus*. The antimicrobial activity of NER is associated with the hydrophobic characteristic of the molecule, preventing the affinity with the cytoplasmic membrane of bacteria. Thus, the interaction between NER and the bacterial membrane changes the permeability of the last one, allowing the leakage of potassium ions ($K^+$). It causes the rupture of the membrane, resulting in the death of the bacteria. The rupture of the bacterial membrane caused by NER is similar to the mechanism observed for terpene alcohols, explaining the inhibition of microorganism proliferation.

The results confirm that the fibrous mats containing nerolidol were effective for the control of Gram-positive and Gram-negative microorganisms Hence, they would be potentially suitable for wound-dressing purposes. In this case, they could decrease the chances of contact-contracted bacterial infections. However, performing these tests and other *in vivo* relevant analyses (like *in vivo* degradation, for example) are still prospects of this work.

*In vitro* stability

The stability of the PVA/NERx nanofibers was assessed using an aqueous medium. Figure 5 portrays the stability in terms of the percentage of mass loss. The results confirm that NER had a positive influence on the stability of the PVA/NER25 fibers, leading to a mass loss of ($19.4 \pm 2.57$)%. The results suggest that 25% of NER allows the system (polymer solution + electrospinning conditions) to reach a stability condition that leads to the formation of

**Table 4.** The diameter of the inhibition zone of the PVA/NERx samples compared to positive controls (penicillin (PEN) and chloramphenicol (CLO))

| Treatment | | Diameter of the inhibition zone / mm | | |
|---|---|---|---|---|
| | | *Staphylococcus epidermidis* | *Staphylococcus aureus* | *Pseudomonas aeruginosa* |
| Antibiotic | PEN 10 µg | $10.0 \pm 0.00^a$ | $8.50 \pm 1.20^a$ | $38.5 \pm 0.10^a$ |
| | CLO 30 µg | $27.5 \pm 0.40^b$ | $23.0 \pm 0.00^b$ | $11.0 \pm 1.60^b$ |
| Fibrous mats | PVA/NER0 | $0.00 \pm 0.00$ | $0.00 \pm 0.00$ | $0.00 \pm 0.00$ |
| | PVA/NER25 | $12.0 \pm 3.60^a$ | $10.7 \pm 1.20^a$ | $14.3 \pm 0.60^c$ |
| | PVA/NER50 | $21.3 \pm 0.60^c$ | $14.0 \pm 1.80^c$ | $17.3 \pm 0.60^d$ |

For each column, (mean ± SD) that do not share the same letter are statistically different at 95%. The values were standardized to three significant figures.

thinner fibers (the PVA/NER25 fibers were the thinnest ones among all samples). Moreover, the physical interaction between PVA and NER probably contributed to holding the structure even when exposed to the aqueous medium.
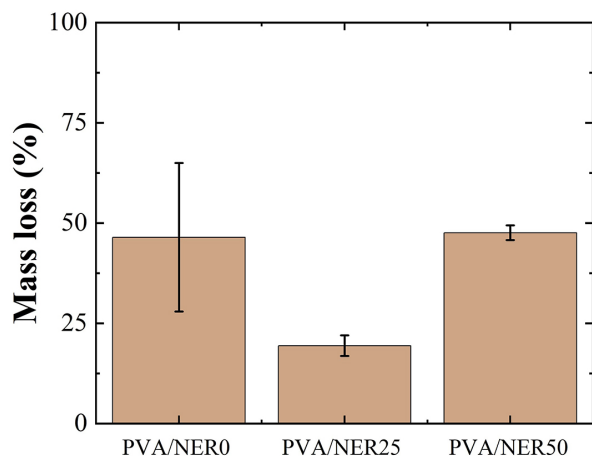


**Figure 5.** *In vitro* stability of the PVA/NERx fibers in aqueous medium.

Although PVA is a water-soluble polymer, it only solubilizes if the solution is at a high temperature.[27] Therefore, the mass losses observed in Figure 5 were not supposed to be the result of the dissolution of PVA in the aqueous medium, especially because the analysis was performed at T = 35 °C. Nevertheless, judging by the similar mass losses observed for PVA/NER0 ((46.4 ± 18.5)%) and PVA/NER50 ((47.6 ± 1.86)%), the mass loss could not be the result of an eventual release of NER into the medium.

It is possible that PVA had polymer chains of different lengths and, consequently, molecular weights. Low-molecular-weight chains are more likely to be water-soluble than high-molecular-weight chains. Thus, the obtained results could be an indicator of the presence of PVA oligomers in the fibers. These oligomers probably formed stronger interactions with the aqueous medium and leached from the matrix, justifying the observed mass losses. It corroborates the positive interaction between PVA and 25% of NER, and corroborates the SEM results (Figure 1).

Despite losing almost half of its initial mass, wound dressings are usually replaced by new ones within less than 24 h. Hence, the mass loss observed for the PVA/NERx fibers would represent an issue regarding their potential use as a wound dressing.

## Conclusions

The electrospinning technique was used to produce fibrous mats composed of poly(vinyl alcohol) (PVA) and the antimicrobial agent nerolidol. The SEM results confirmed the formation of homogeneous nanofibers for PVA/NER0.

However, the incorporation of NER probably prevented the complete solvent evaporation of the solvent. It consequently led to the coalescence of the fibers, becoming more evident for the fibers containing the highest amount of NER (PVA/NER50). NER also affected the diameter of the fibers: it increased the diameter from (656 ± 76.4) nm to (901 ± 193) nm for PVA/NER0 and PVA/NER50, respectively, but the PVA/NER25 fibers were the thinnest ones ((583 ± 144) nm).

Physical-chemical characterizations confirmed the interaction between PVA and NER. Since they have opposite polarities, the interactions mostly involved the non-polar portions of the precursors, leading to the formation of van der Waals and potentially London interactions between them. Nonetheless, the FTIR results also suggest the formation of hydrogen interactions between the polar groups from both precursors.

The incorporation of NER also increased the hydrophobic character of the fibers. The contact angles increased as the amount of NER increased, confirming that NER molecules were part of the outer part of the fibers. DSC and TG/DTG analyses confirmed that the incorporation of NER decreased the crystallinity and thermal stability of the fibers. However, while the thermal stability decrease depended on the amount of NER added to the fibers, the crystallinity degree was not proportionally affected by it. The percentage of crystallinity of the fibers decreased from 10.0% to ca. 6.50%.

*In vitro* antimicrobial analysis showed that the fibrous mats efficiently inhibited the proliferation of Gram-positive and Gram-negative bacteria due to the presence of nerolidol in the membranes. In some cases, the PVA/NER50 fibers were even more efficient than the antibiotics used as controls. These results indicate that the PVA/NERx mats are potentially suitable for wound-dressing purposes. Even though PVA/NER0 and PVA/NER50 were not very stable in the aqueous medium, it would not compromise their potential use as a wound dressing. However, *in vivo* assays are necessary to confirm the previous statement, and it is a prospect of this work.

## Acknowledgments

### Author Contributions

Paola Amanda P. Machado was responsible for data curation, formal analysis, investigation, resources, visualization, writing original draft,

Machado *et al.*

writing-review and editing; Gabriel N. Fraga for data curation, formal analysis, investigation, writing original draft, writing-review and editing; Alessandra R. Medeiros for data curation, formal analysis, resources, software, writing-review and editing; Michelly Cristina G. Pellá for data curation, investigation, writing original draft, writing-review and editing; Nelson B. Colauto for data curation, formal analysis, investigation, writing original draft; Giani Andrea Linde for data curation, formal analysis, investigation, writing original draft; Fernando N. Cavalheiro for data curation, investigation; Maria Graciela I. Faria for data curation, formal analysis, investigation, writing original draft; Douglas C. Dragunski for conceptualization, data curation, formal analysis funding acquisition, investigation, project administration, resources, software, validation, visualization, writing original draft, writing-review and editing; Josiane Caetano for conceptualization, data curation, formal analysis funding acquisition, investigation, project administration, resources, software, validation, visualization, writing original draft, writing-review and editing.

## References

1. Pellá, M. C. G.; Simão, A. R.; Lima-Tenório, M. K.; Tenório-Neto, E.; Scariot, D. B.; Nakamura, C. V.; Rubira, A. F.; *Carbohydr. Polym.* **2020**, *239*, 116236. [Crossref]

2. Pellá, M. C. G.; Simão, A. R.; Lima-Tenório, M. K.; Scariot, D. B.; Nakamura, C. V.; Muniz, E. C.; Rubira, A. F.; *Carbohydr. Polym.* **2020**, *250*, 116879. [Crossref]

3. Simão, A. R.; Fragal, V. H.; Lima, A. M. O.; Pellá, M. C. G.; Garcia, F. P.; Nakamura, C. V.; Tambourgi, E. B.; Rubira, A. F.; *Int. J. Biol. Macromol.* **2020**, *148*, 302. [Crossref]

4. Bilirgen, A. C.; Toker, M.; Odabas, S.; Yetisen, A. K.; Garipcan, B.; Tasoglu, S.; *ACS Biomater. Sci. Eng.* **2021**, *7*, 926. [Crossref]

5. Yahya, E. B.; Amirul, A. A.; Abdul, H. P. S. A.; Olaiya, N. G.; Iqbal, M. O.; Jummaat, F.; Sofea, A. K. A.; Adnan, A. S.; *Polymers* **2021**, *13*, 1612. [Crossref]

6. Pellá, M. C. G.; Silva, O. A.; Pellá, M. G.; Beneton, A. G.; Caetano, J.; Simões, M. R.; Dragunski, D. C.; *Food Chem.* **2020**, *309*, 125764. [Crossref]

7. Silva, O. A.; Pellá, M. G.; Pellá, M. G.; Caetano, J.; Simões, M. R.; Bittencourt, P. R. S.; Dragunski, D. C.; *Int. J. Biol. Macromol.* **2019**, *128*, 290. [Crossref]

8. Francisco, C. B.; Pellá, M. G.; Silva, O. A.; Raimundo, K. F.; Caetano, J.; Linde, G. A.; Colauto, N. B.; Dragunski, D. C.; *Int. J. Biol. Macromol.* **2020**, *152*, 272. [Crossref]

9. Hardt, J. C.; Galdioli Pellá, M. C.; Meira, A. C. R.; Giombelli Rosenberger, A.; Caetano, J.; Dragunski, D. C.; *J. Mol. Liq.* **2021**, *339*, 116694. [Crossref]

10. Antunes, L. R.; Breitenbach, G. L.; Pellá, M. C. G.; Caetano, J.; Dragunski, D. C.; *Int. J. Biol. Macromol.* **2021**, *182*, 333. [Crossref]

11. Kamoun, E. A.; Kenawy, E. R. S.; Chen, X.; *J. Adv. Res.* **2017**, *8*, 217. [Crossref]

12. Cantin-Warren, L.; Guignard, R.; Cortez Ghio, S.; Larouche, D.; Auger, F.; Germain, L.; *J. Funct. Biomater.* **2018**, *9*, 53. [Crossref]

13. Ding, Q.; Wang, Z.; Hu, Y.; Dong, Z.; Chen, J.; Zhou, Q.; Li, H.; Tang, S.; *Carbohydr. Polym.* **2022**, *292*, 119698. [Crossref]

14. Li, H.; Cheng, F.; Orgill, D. P.; Yao, J.; Zhang, Y. S.; *Essays Biochem.* **2021**, *65*, 533. [Crossref]

15. Yue, Y.; Gong, X.; Jiao, W.; Li, Y.; Yin, X.; Si, Y.; Yu, J.; Ding, B.; *J. Colloid Interface Sci.* **2021**, *592*, 310. [Crossref]

16. Xia, J.; Zhang, H.; Yu, F.; Pei, Y.; Luo, X.; *ACS Appl. Mater. Interfaces* **2020**, *12*, 24370. [Crossref]

17. Chen, K.; Pan, H.; Ji, D.; Li, Y.; Duan, H.; Pan, W.; *Mater. Sci. Eng., C* **2021**, *127*, 112245. [Crossref]

18. Castro, K. C.; Campos, M. G. N.; Mei, L. H. I.; *Int. J. Biol. Macromol.* **2021**, *173*, 251. [Crossref]

19. Liu, Y.; Li, T.; Han, Y.; Li, F.; Liu, Y.; *Curr. Opin. Biomed. Eng.* **2021**, *17*, 100247. [Crossref]

20. Rosenberger, A. G.; Pellá, M. C. G.; Medeiros, A. R.; Lima, F. S.; Fraga, G. N.; Caetano, J.; Dragunski, D. C. In *Nanoengineering of Biomaterials*; Sougata, J.; Subrata, J., eds.; Wiley: Hoboken, 2022, ch. 4.

21. Pires, A. L. R.; Bierhalz, A. C. K.; Moraes, Â. M.; *Quim. Nova* **2015**, *38*, 957. [Crossref]

22. Bosworth, L.; Downes, S.; *Electrospinning for Tissue Regeneration*; Elsevier Science: London, UK, 2011.

23. Zagho, M. M.; Elzatahry, A. In *Electrospinning: Material, Techniques, and Biomedical Applications*; Haider, S.; Haider, A.; IntechOpen: Rijeka, Croatia, 2016, ch. 1.

24. Augustine, R.; Hasan, A.; Yadu Nath, V. K.; Thomas, J.; Augustine, A.; Kalarikkal, N.; Al Moustafa, A.-E.; Thomas, S.; *J. Mater. Sci. Mater. Med.* **2018**, *29*, 163. [Crossref]

25. Augustine, R.; ur Rehman, S. R.; K. S., J.; Hasan, A.; *RSC Adv.* **2021**, *11*, 572. [Crossref]

26. Luo, F.-L.; Nagel, K. A.; Zeng, B.; Schurr, U.; Matsubara, S.; *Ann. Bot.* **2009**, *104*, 1435. [Crossref]

27. Tamai, Y.; Tanaka, H.; Nakanishi, K.; *Macromolecules* **1996**, *29*, 6750. [Crossref]

28. Chan, W.-K.; Tan, L. T. H.; Chan, K.-G.; Lee, L.-H.; Goh, B.-H.; *Molecules* **2016**, *21*, 529. [Crossref]

29. Ali, B.; Al-Wabel, N. A.; Shams, S.; Ahamad, A.; Khan, S. A.; Anwar, F.; *Asian Pac. J. Trop. Biomed.* **2015**, *5*, 601. [Crossref]

30. Tao, R.; Wang, C.-Z.; Kong, Z.-W.; *Molecules* **2013**, *18*, 2166. [Crossref]

31. Arruda, D. C.; D'Alexandri, F. L.; Katzin, A. M.; Uliana, S. R. B.; *Antimicrob. Agents Chemother.* **2005**, *49*, 1679. [Crossref]

32. Krist, S.; Banovac, D.; Tabanca, N.; Wedge, D. E.; Gochev, V. K.; Wanner, J.; Schmidt, E.; Jirovetz, L.; *Nat. Prod. Commun.* **2015**, *10*, 143. [Crossref]

33. Rasband, W. S.; *ImageJ*; U. S. National Institutes of Health, Bethesda, Maryland, USA, 2021. [Link] accessed in May 2023

34. Kong, Y.; Hay, J. N.; *Polymer* **2002**, *43*, 3873. [Crossref]

35. Nishio, Y.; Haratani, T.; Takahashi, T.; Manley, R. S. J.; *Macromolecules* **1989**, *22*, 2547. [Crossref]

36. Clinical and Laboratory Standards Institute (CLSI); CLSI document M100-S29, *Performance Standards for Antimicrobial Susceptibility Testing*, 29th Informational Supplement; Clinical and Laboratory Standards Institute: Wayne, PA, 2019.

37. *Minitab Inc.*, version 19; State College, PA, USA, 2021. [Link] accessed in May 2023

38. Ullah, S.; Hashmi, M.; Hussain, N.; Ullah, A.; Sarwar, M. N.; Saito, Y.; Kim, S. H.; Kim, I. S.; *J. Water Process Eng.* **2020**, *33*, 101111. [Crossref]

39. Bunn, C. W.; *Nature* **1948**, *161*, 929. [Crossref]

40. Atkins, P.; de Paula, J.; *Elements of Physical Chemistry*; OUP Oxford: Oxford, 2013.

41. Sill, T. J.; von Recum, H. A.; *Biomaterials* **2008**, *29*, 1989. [Crossref]

42. Kishan, A. P.; Cosgriff-Hernandez, E. M.; *J. Biomed. Mater. Res., Part A* **2017**, *105*, 2892. [Crossref]

43. Haider, A.; Haider, S.; Kang, I.-K.; *Arabian J. Chem.* **2018**, *11*, 1165. [Crossref]

44. Bruni, G. P.; de Oliveira, J. P.; Gómez-Mascaraque, L. G.; Fabra, M. J.; Guimarães Martins, V.; Zavareze, E. R.; López-Rubio, A.; *Food Packag. Shelf Life* **2020**, *23*, 100426. [Crossref]

45. Pavia, D. L.; Lampman, G. M.; Kriz, G. S.; Vyvyan, J. A.; *Introduction to Spectroscopy*; Cengage Learning: Belmont, 2008.

46. Mansur, H. S.; Sadahira, C. M.; Souza, A. N.; Mansur, A. A. P.; *Mater. Sci. Eng., C* **2008**, *28*, 539. [Crossref]

47. Bruice, P. Y.; *Organic Chemistry*; Pearson: Upper Saddle River, 2017.

48. Solomons, T. W. G.; Fryhle, C. B.; Snyder, S. A.; *Organic Chemistry*; Wiley: Hoboken, 2016.

49. Wen, L.; Liang, Y.; Lin, Z.; Xie, D.; Zheng, Z.; Xu, C.; Lin, B.; *Polymer* **2021**, *230*, 124048. [Crossref]

50. Qin, X.; Dou, G.; Jiang, G.; Zhang, S.; *J. Ind. Text.* **2012**, *43*, 34. [Crossref]

51. Van Etten, E. A.; Ximenes, E. S.; Tarasconi, L. T.; Garcia, I. T. S.; Forte, M. M. C.; Boudinov, H.; *Thin Solid Films* **2014**, *568*, 111. [Crossref]

52. Watase, M.; Nishinari, K.; *J. Polym. Sci.* **1985**, *23*, 1803. [Crossref]

53. Peppas, N. A.; Merrill, E. W.; *J. Appl. Polym. Sci.* **1976**, *20*, 1457. [Crossref]

54. Patel, A. K.; Bajpai, R.; Keller, J. M.; *Microsyst. Technol.* **2014**, *20*, 41. [Crossref]

55. de Souza, E. P. B. S. S.; Gomes, M. V. L. D.; Lima, B. S.; Silva, L. A. S.; Shanmugan, S.; Cavalcanti, M. D.; de Albuquerque Jr., R. L. C.; Carvalho, F. M. S.; Marreto, R. N.; de Lima, C. M.; Júnior, L. J. Q.; Araújo, A. A. S.; *Life Sci.* **2021**, *265*, 118742. [Crossref]

56. Sonker, A. K.; Rathore, K.; Nagarale, R. K.; Verma, V.; *J. Polym. Env.* **2018**, *26*, 1782. [Crossref]

57. Tampau, A.; González-Martínez, C.; Chiralt, A.; *React. Funct. Polym.* **2020**, *153*, 104603. [Crossref]